GSA Data Repository item 2011051

Supplementary Data and Discussion, Tables, Figures, and References

Whiteside and Ward

"Ammonid diversity and disparity track episodes of chaotic carbon during the early Mesozoic"

Source of Diversity Data represented in Figure 1: To reduce errors introduced by inaccurate global stratigraphic correlation, inconsistent taxonomy between regions, and monographic effects, we compiled a regional dataset of ammonoid diversity from western North America. To minimize discrepancy between taxonomic authorities, we endeavored to use ammonoid taxonomic compendia produced by a low number of individual taxonomists. This study was greatly aided in that all Triassic data presented here (the majority of taxa examined) were recognized and defined by a single worker (Tozer, 1994). Similarly, Permian ammonoid diversity and occurrences were compiled from Nassichuk (1970, 1971, 1977) and Miller et al., (1957). For the Jurassic, we collated data from Guex (1995), Guex et al. (2004), Pálfy et al. (1994), and Taylor (1998).

Discussion of Isotopic Data in Figure 1: The carbon isotopic curve displayed in Fig. 1 of the manuscript was comprised of data from Payne et al. (2004), Muttoni et al. (2004), and van de Schootbrugge et al. (2008). Currently, there is no available published carbonate data for most of the Carnian. Although published $\delta^{13}C_{carb}$ data for the Rhaetian

of Queen Charlotte Islands, British Columbia exists (Ward et al., 2004), most if not all samples had been diagenetically altered, so we could not include this data. Furthermore, the limited stratigraphic sampling of an early Rhaetian $\delta^{13}C_{carb}$ dataset from Austria (Krystyn et al., 2007) makes it difficult to correlate with any confidence to the Triassic timescale.

Diversity Residuals Data and Discussion: Generic diversity was plotted against number of occurrences for each time bin (Fig. DR1). A linear regression was calculated from these data and this was used to calculate the residuals for each diversity data point (Table DR1).

The predominance of positive and negative residuals, lack of values equal to zero, and low correlation coefficient (R^2=0.57; Fig. DR1) indicate that sampling (number of occurrences) has a minimal effect on the shape of our diversity curve. In particular, the residual data indicate that the Early Triassic and Triassic-Jurassic boundary diversity minima and Middle-Late Triassic maxima are robust signals when accounting for sampling intensity.

New $\delta^{13}C_{org}$ Data Presented in Figure 2: The late Norian data shown in Fig. 2 from the main text is based on three measured sections (Table DR2) sampled at 1-2 m intervals from Frederick Island, Queen Charlotte Islands, British Columbia, Canada.
In Fig. 2, section FI2 is dark red, section FI3 is green, and section FI4 is red. The three sections were correlated to each other using a local marker bed informally named the “FB limestone”, approximately 34 meters below the LAD of *Monotis*. These three

stratigraphic sections were placed in the greater Queen Charlotte Islands stratigraphy based on the presence of *Halobia* sp. and overlying well-bedded coquinas filled with *Monotis* spp. Ammonoids were exceedingly common over most of this interval (more common, in fact, than anywhere else on Frederick Island), where the lowest part of the continuous stratigraphic section is lower Norian in age based on ammonoids and bivalves. Within 10 m of the *Monotis* beds, however, there is a drastic fall-off of ammonoid abundance to near 0 in the lowest *Monotis* beds.

Samples for organic carbon $^{13}C/^{12}C$ analysis were acidified with 20 μl of 50% HCl to remove carbonate, oven-dried at 50 °C, and measured at the stable isotope laboratory at the University of Washington on a ThermoFinnigan DELTAplus mass spectrometer via a ThermoFinnigan CONFLO III interface. Values are corrected with standard methods and reported relative to the Vienna PDB. The analytical precision for this analysis, based on replicate analyses, is estimated at 0.08‰. Raw values are listed in Table DR2.

Morphotype Data for Early Mesozoic Ammonoids of Western North America: Each of the Upper Permian through Hettangian ammonoid genera examined for this study was identified as belonging to one of six morphotypes (Tables DR3-S4; Fig. DR2). Oxycones are shells with high whorl expansion rate (W), low whorl shape (S), very low shell overlap (D), and short body chambers (<100º). All of these attributes are consistent with interpretations that these particular shell types had evolved to become strong and fast swimmers (Saunders et al., 1999). Normal shells have intermediate W, D, and S, and moderate to weak ornament; ornamented morphs display strong ornament (Jacobs et al.,

1994); serpenticones have low W, high D, variable sutures (S), extremely long body chambers (>180^{o}), and low (or none) to only moderate ornamentation; and heteromorphs, which also have long body chambers but depart from normal planispiral ornamentation. In the Late Triassic and early Hettangian, the most common heteromorphic forms were either torted (snail like) or openly coiled forms that were both relatively small even as adults, and probably would have been poor swimmers (Ward, 1979; Fig. DR2). Depressed shells have intermediate to high W, intermediate D, and high S.

Functional Redundancy as Applied to Post-Extinction Ecosystems: Functional redundancy is when multiple taxa serve overlapping functions in the same ecosystem. This can include sharing similar trophic links with predators and prey. Modelling of both modern and fossil ecosystems demonstrate that ecosystems with high levels of redundancy are the most stable and resistant to perturbation, whereas ecosystems with little or no redundancy and few overlapping trophic links, are subject to cyclical variation and possible collapse (MacArthur, 1955; Roopnarine et al., 2007).

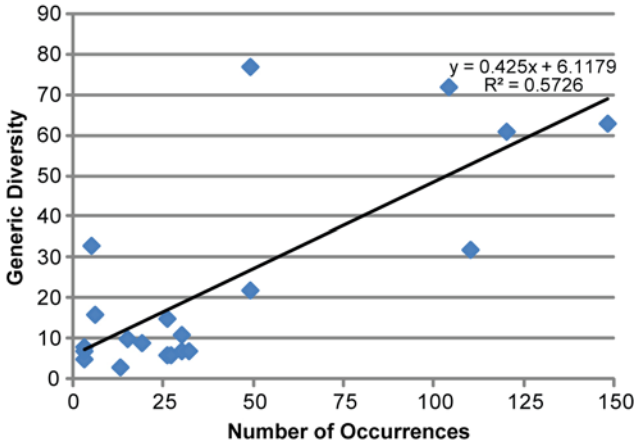

Figure DR1. Linear regression of generic diversity vs. number of occurrences. Each data point represents a single time bin in our analysis.

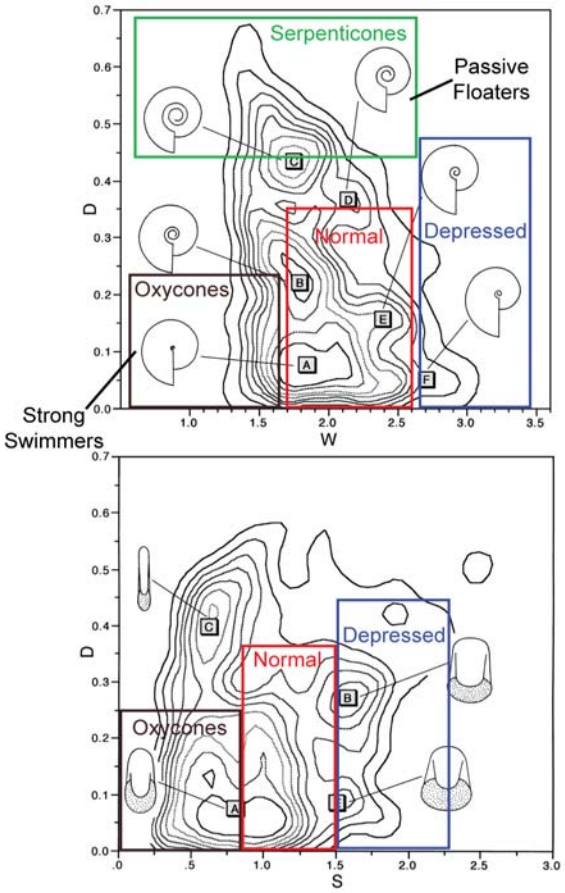

Figure DR2. Ammonoid morphotypes as represented by whorl expansion (W), whorl overlap (D), and whorl shape (S) morphospace [original figure from Saunders et al. (2004)]. Top, illustrations of modal geometries in ammonoid genera. Bottom, primary modal geometries shown in D-S density contours with representative apertural views.

Table DR1. Record of ammonoid generic level diversity and residual data for Pacific Coast of North America.

Time Bin	Raw Diversity	Occurrences	Diversity Residuals
Lower Griesbachian	7	30	-4.27
Upper Griesbachian	7	32	-4.58
Lower Dienerian (Candidus Zone)	6	26	-4.02
Upper Dienerian (Sverdruipi Zone)	11	30	-2.83
Middle Smithian (Romunderi Zone)	15	26	-0.78
Upper Smithian (Tardus Zone)	9	19	-1.87
Lower Spathian (Pilaticus Zone)	5	3	-0.86
Upper Spathian (Subcobustus Zone)	6	27	-4.17
Lower Anisian	22	49	-1.78
Upper Anisian	77	49	18.01
Ladinian	61	120	1.40
Carnian	32	110	-7.51
Lower Norian	72	104	7.80
Upper Norian	63	148	-2.17
Rhaetian (Amoneum)	10	15	-0.90
Rhaetian (Crickmayi)	3	13	-3.11
Lowest Hettangian	7	3	-0.14
Lower Hettangian	8	3	0.22
Upper Hettangian	16	6	2.64
Sinemurian	33	5	8.91

Table DR2. Late Norian $\delta^{13}C_{org}$ data from Frederick Island, Queen Charlotte Islands. Stratigraphic position is based on number of meters below the Triassic-Jurassic boundary. This boundary in the Queen Charlotte Islands is identified at a major turnover of radiolarian species, correlative with the top of the Crickmayi ammonoid zone (Ward et al., 2004). No values for standard deviation indicate there were not enough successful replicates to calculate this value. Abbreviations: TOC, total organic carbon.

Section	Sample ID	Stratigraphic Position (m)	Average TOC	TOC Standard Deviation	$\delta^{13}C_{org}$ Average	$\delta^{13}C_{org}$ Standard Deviation
FI3	318	-130.5	0.068		-29.13	0.00
FI3	317	-131.0	0.055	0.021	-29.14	0.20
FI3	316	-131.5	0.124		-29.51	0.10
FI3	315	-132.4	0.042	0.017	-29.01	0.20
FI3	314	-133.2	0.039	0.018	-29.12	0.26
FI3	313	-134.5	0.047	0.019	-29.39	0.03
FI3	312	-134.9	0.059	0.025	-29.50	0.15
FI3	311	-135.3	0.056	0.024	-29.81	0.09
FI3	310	-135.7	0.043	0.021	-29.10	0.42
FI3	309	-136.2	0.038	0.020	-29.31	0.23
FI3	308	-137.5	0.054	0.025	-29.28	0.29
FI3	307	-138.2	0.084	0.017	-28.96	0.18
FI3	306	-139.0	0.064	0.031	-29.51	0.30
FI3	305	-139.5	0.050	0.019	-29.49	0.19
FI3	304	-139.5	0.068	0.034	-29.52	0.23
FI3	303	-140.4	0.023	0.016	-28.92	0.23
FI3	302	-141.7	0.042	0.018	-29.21	0.00
FI3	301	-142.4	0.045	0.011	-29.60	0.29
FI4	21.5	-143.3	0.056	0.007	-29.71	0.21
FI4	26.5	-145.3	0.036	0.007	-28.93	0.35
FI4	29	-146.5	0.035		-28.75	
FI4	33.5	-148.0				
FI4	36.5	-149.2	0.039		-28.48	
FI4	38.5	-150.2				
FI4	39.5	-150.6	0.052		-28.54	
FI4	44.5	-152.6	0.041	0.000		
FI4	45	-152.8	0.010		-28.42	
FI4	49	-154.5	-0.011	0.023	-28.00	0.44
FI4	54	-156.5	0.015			
FI4	58.2	-158.4	-0.017			
FI4	58.6	-158.6	0.009	0.012	-28.59	0.28
FI4	59.5	-159.0	0.010			

FI4	60.1	-159.4	0.004		-28.87	
FI4	60.4	-159.5	0.013		-28.66	
FI4	60.7	-159.7				
FI4	62	-160.3				
FI4	63	-160.8	0.004		-28.32	
FI4	66	-162.4	0.023		-28.98	
FI4	68	-163.6	0.011		-29.76	
FI4	80	-171.6	0.015			
FI4	81.3	-172.4	0.043		-29.76	
FI4	85	-174.5	0.014		-30.22	
FI4	86.6	-175.4	0.003		-28.09	
FI4	89.2	-176.6	0.013		-28.56	
FI4	92.4	-178.1				
FI4	94.8	-179.0				
FI4	98	-180.6	0.016		-28.04	
FI4	101	-182.1				
FI4	103	-183.0	0.037	0.006	-27.84	0.16
FI4	105	-184.0	0.021		-27.56	
FI4	108.7	-185.8	0.019	0.001	-27.84	0.40
FI4	110.5	-186.7				
FI4	111.1	-186.9	0.032		-28.16	
FI4	112	-187.4	0.026	0.006	-28.47	0.74
FI4	113.5	-188.0	0.015		-28.05	
FI4	114.8	-188.8	0.023		-27.48	
FI4	115.9	-189.3	0.033		-28.19	
FI4	117.1	-189.9	0.034	0.001	-28.44	0.10
FI4	118.4	-190.5	0.007	0.001	-29.02	0.22
FI4	119.1	-190.9	0.022		-29.04	
FI4	120.9	-191.8	0.013	0.000	-29.27	0.10
FI4	122.2	-192.4	0.023		-29.17	
FI4	123	-192.8				
FI4	125.8	-194.2	0.019	0.003	-29.03	0.06
FI4	126.8	-194.7	0.032	0.001	-29.02	0.09
FI4	128.1	-195.4	0.012		-29.35	
FI4	128.3	-195.5				
FI4	129.2	-195.9	-0.003		-28.90	
FI4	129.8	-196.2	0.013		-28.92	
FI4	131.5	-197.1	0.010	0.021	-29.21	0.16
FI4	134	-198.3	-0.013		-29.32	
FI4	136	-199.3	0.021		-28.78	
FI4	138	-200.3	0.002		-29.19	
FI4	139.8	-201.2				
FI4	142.6	-202.7	0.045		-29.09	

FI4	143.5	-203.1	0.010		-29.10	
FI4	144.3	-203.5	0.010		-29.09	
FI4	146.1	-204.4	0.038		-29.30	
FI4	148.3	-205.6	0.029	0.009	-28.98	0.16
FI4	149.6	-206.2				
FI4	150.8	-206.8	0.017		-28.41	
FI4	152	-207.5	0.028		-29.14	
FI4	154.2	-208.6	0.038	0.000	-29.42	0.04
FI4	155.4	-209.2	0.023		-28.79	
FI4	156.1	-209.5	-0.017		-28.41	
FI4	157.1	-209.6	0.004	0.002	-28.68	0.04
FI4	159.2	-210.3	0.001		-28.83	
FI4	161	-210.8				
FI4	164.2	-211.8	0.012		-28.94	
FI4	165.9	-212.4	0.029		-28.95	
FI4	167.9	-213.2	0.004		-28.57	
FI4	169.5	-213.8	0.049		-28.94	
FI4	171.5	-214.7	0.014	0.004	-28.80	0.05
FI4	174	-215.8	0.004	0.016	-28.27	0.02
FI4	175.8	-216.5	0.009		-28.29	
FI4	177.8	-217.3	0.058	0.006	-28.78	0.05
FI4	179	-217.7	-0.006	0.007	-28.54	0.05
FI4	180	-218.1	0.005	0.007	-28.46	0.06
FI2	225	-175.3	0.046	0.009	-28.75	0.33
FI2	224	-176.3	0.038	0.005	-28.91	0.44
FI2	223	-177.0	0.026	0.005	-28.86	0.18
FI2	222	-177.6	0.032	0.005	-28.91	0.53
FI2	221	-177.8	0.026	0.005	-28.66	0.18
FI2	220	-179.5	0.034	0.006	-29.01	0.39
FI2	201	-180.3	0.018	0.002	-28.64	0.27
FI2	202	-181.3	0.020	0.003	-28.30	0.13
FI2	203	-181.9	0.043	0.006	-28.83	0.22
FI2	204	-182.3	0.045	0.007	-28.64	0.24
FI2	205	-182.9	0.034	0.005	-28.53	0.24
FI2	207	-183.8	0.033		-27.89	
FI2	208	-184.2	0.045	0.015	-27.81	0.30
FI2	209	-184.7	0.054	0.006	-27.97	0.22
FI2	210	-185.1	0.042	0.004	-27.84	0.17
FI2	211	-185.8	0.042	0.006	-27.67	0.15
FI2	212	-186.2	0.019	0.004	-27.64	0.09
FI2		-186.2	0.030	0.011	-28.05	0.67
FI2	213	-186.5	0.034	0.004	-28.11	0.19

FI2	214	-187.2	0.025	0.004	-27.88	0.07
FI2	215	-187.9	0.043	0.010	-28.15	0.21
FI2	216	-188.2	0.049	0.008	-27.68	0.19
FI2	217	-188.7	0.019	0.004	-27.37	0.23
FI2	218	-188.9	0.052	0.004	-28.47	0.13
FI2	227	-190.5	0.035	0.005	-28.14	0.20
FI2	228	-191.6	0.020	0.006	-28.99	0.26
FI2	229	-192.3	0.034	0.003	-28.58	0.15
FI2	230	-193.2	0.045	0.006	-28.47	0.42
FI2	231	-193.9	0.026	0.032	-29.06	0.34
FI2	232	-195.1	0.032	0.017	-29.25	0.00
FI2	233	-195.8	0.026	0.002	-29.26	0.20
FI2	234	-196.3	0.045	0.002	-29.10	0.35
FI2	235	-196.9	0.028	0.003	-29.28	0.32
FI2	236	-197.3	0.038	0.012	-29.50	0.16
FI2	237	-197.6	0.041	0.021	-29.29	0.15
FI2	238	-197.9	0.035	0.017	-28.94	0.47
FI2	239	-197.8	0.018		-29.17	
FI2	240	-198.6	0.076	0.018	-29.26	0.27
FI2	241	-198.8	0.055	0.030	-28.97	0.68
FI2	251	-201.5	0.030	0.013	-28.50	0.35
FI2	252	-202.3	0.057	0.029	-28.88	0.66
FI2	253	-203.3	0.047	0.021	-29.03	0.42
FI2	254	-204.4				
FI2	255	-205.2	0.046	0.012	-29.05	0.24
FI2	256	-206.0	0.047	0.022	-28.91	0.55
FI2	257	-206.7	0.050	0.026	-28.74	0.71
FI2	258	-207.9	0.055	0.024	-28.73	0.67

Table DR3. Specific attributes for each morphotype defined in this paper.

Shell coiling descriptors (W,D,S)	**Oxycone**	**Normal**	**Depressed**	**Ornamented**	**Serpenticone**	**Heteromorphic**
W	1.3-3	1.5- 2.5	1.3-3	Any	1.2-2.0	Any
D	0-.2	.2-.5	.1-.5	Any	.4-.7	NA
S	0-.5	.6-1.6	1.2-2.5	Any	.5-1.5	any

Table DR4. Number of genera assigned to each morphotype from the earliest Triassic through the Early Jurassic.

	Oxycone	Normal	Depressed	Ornamented	Serpenticone	Heteromorph
Lower Griesbachian	4	1	0	0	2	0
Upper Griesbachian	4	3	0	0	0	0
Lower Dienerian	4	2	0	0	0	0
Upper Dienerian	7	4	0	0	0	0
Lower Smithian	7	4	2	0	2	0
Upper Smithian	1	5	0	2	1	0
Lower Spathian	2	2	1	0	0	0
Upper Spathian	3	2	0	0	1	0
Lower Anisian	14	5	1	2	0	0
Upper Anisian	24	12	10	25	6	0
Ladinian	21	8	8	20	4	0
Carnian	10	5	2	11	4	0
Lower Norian	26	7	2	10	2	0
Upper Norian	21	5	5	16	5	0
Lower Rhaetian	1	3	1	2	0	3
Upper Rhaetian	0	2	0	0	0	1
Lower Hettangian	12	1	0	2	0	2
Upper Hettangian	0	1	0	0	6	1
Sinemurian	2	2	1	0	5	0

References

Guex, J., 1995, Ammonites hettangiennes de la Gabbs Valley Range (Nevada, USA): Mémoires de Géologie (Lausanne), v. 27, p. 1-131.

Guex J., Bartolini, A., Atudorei, V., and Taylor, D., 2004, High-resolution ammonite and carbon isotope stratigraphy across the Triassic- Jurassic boundary at New Cork Canyon (Nevada): Earth and Planetary Science Letters , v. 225, p. 29–41.

Jacobs, D., Landman, N., and Chamberlain, J., 1994, Ammonite shell shape covaries with facies and hydrodynamics: Iterative evolution as a response to changes in basinal environment: Geology v. 22, p. 905-908.

Krystyn, L., Richoz, S., Gallet, Y., Bouquerei, H., and Kürschner, W., 2007, Updated bio- and magnetostratigraphy from Steinbergkogel (Austria), candidate GSSP for the base of the Rhaetian stage: Albertiana, v. 36, p. 164-173.

MacArthur, R., 1955, Fluctuations of animal populations and a measure of community stability: Ecology, v. 36, p. 533-536.

Miller, A.K., Furnish, W.M., and Clark, D.L., 1957, Permian ammonoids from western United States: Journal of Paleontology, v. 31, p. 1057-1068.

Muttoni, G., Kent, D.V., Olsen, P.E., Distefano, P., Lowrie, W., Bernasconi, S., and Hernandez, F.M., 2004, Tethyan magnetostratigraphy from Pizzo Mondello (Sicily) and correlation to the Late Triassic Newark astrochronological polarity time scale: Geological Society of America Bulletin 116, p.1043-1058.

Nassichuk, W.W., 1970, Permian ammonoids from Devon and Melville Islands, Canadian Arctic Archipelago: Journal of Paleontology, v. 44, p. 77-97.

Nassichuk, W.W., 1971, Permian ammonoids and nautiloids, southeastern Eagle Plain,

Yukon Territory: Journal of Paleontology, v. 45, p. 1001-1021.

Nassichuk, W.W., 1977, Upper Permian ammonoids from the Cache Creek Group in western Canada: Journal of Paleontology, v. 51, p. 557-590.

Pálfy, J., Smith, P.L., and Tipper, H.W., 1994, Sinemurian (Lower Jurassic) ammonoid biostratigraphy of the Queen Charlotte Islands, western Canada: Geobios, v. 17, p. 385-393.

Payne, J.L., Lehrmann, D.J., Wei, J., Orchard, M.J., Schrag, D.P., and Knoll, A.H., 2004, Large perturbations of the carbon cycle during recovery from the end-Permian extinction: Science, v. 305, p. 506-509.

Roopnarine, P.D., Angielczyk, K.D., Wang, S.C., and Hertog, R., 2007, Trophic network models explain instability of Early Triassic terrestrial communities: Proceedings of the Royal Society B: Biological Sciences, v. 274, no. 1622, p. 2077-2086. doi:10.1098/rspb.2007.0515.

Saunders, W.B., Work, D.M., and Nikolaeva, S.V., 1999, Evolution of complexity in Paleozoic ammonoid sutures: Science, v. 286, p. 760-763.

Saunders, W.B., Work, D.M., and Nikolaeva, S.V., 2004, The evolutionary history of shell geometry in Paleozoic ammonoids: Paleobiology v. 30, p. 19-43.

Taylor, D.G., 1998, Late Hettangian-Early Sinemurian (Jurassic) ammonite biochronology of the Western Cordillera, United States: Geobios, v. 31, p. 467-497.

Tozer, T., 1994, Canadian Triassic ammonoid fauans: Geological Survey of Canada Bulletin 467, 663p.

van de Schootbrugge, B., Payne, J.L., Tomasovych, A., Pross, J., Fiebig, J., Benbrahim, M., Föllmi, K.B., and Quan, T.M., 2008, Carbon cycle perturbation and stabilization

in the wake of the Triassic-Jurassic boundary mass-extinction event: Geochemistry, Geophysics, Geosystems v. 9, doi: 10.1029/2007GC001914.

Ward, P., 1979, Functional morphology of Cretaceous helically-coiled ammonoite shells: Paleobiology v. 5, p. 415-422.

Ward, P.D., Garrison, G.H., Haggart, J.W., Kring, D.A., and Beattie, M.J., 2004, Isotopic evidence bearing on Late Triassic extinction events, Queen Charlotte Islands, British Columbia, and implications for the duration and cause of the Triassic/Jurassic mass extinction: Earth and Planetary Science Letters, v. 224, p. 589-600.